Journal of Theoretical Biology 486 (2020) 110099

Contents lists available at ScienceDirect

Journal of Theoretical Biology

journal homepage: www.elsevier.com/locate/jtb

# A minimal modeling framework of radiation and immune system synergy to assist radiotherapy planning

Ghazal Montaseri[a,b,1], Juan Carlos López Alfonso[a,c,1], Haralampos Hatzikirou[a], Michael Meyer-Hermann[a,b,d,*]

[a] Department of Systems Immunology and Braunschweig Integrated Centre of Systems Biology, Helmholtz Centre for Infection Research, Braunschweig, Germany
[b] Centre for Individualised Infection Medicine (CIIM), Hannover, Germany
[c] Department of Gastroenterology, Hepatology and Endocrinology, Hannover Medical School, Hannover, Germany
[d] Institute of Biochemistry, Biotechnology and Bioinformatics, Technische Universität Braunschweig, Germany

ARTICLE INFO

*Article history:*
Received 22 May 2019
Revised 15 October 2019
Accepted 28 November 2019
Available online 29 November 2019

ABSTRACT

Recent evidence indicates the ability of radiotherapy to induce local and systemic tumor-specific immune responses as a result of immunogenic cell death. However, fractionation regimes routinely used in clinical practice typically ignore the synergy between radiation and the immune system, and instead attempt to completely eradicate tumors by the direct lethal effect of radiation on cancer cells. This paradigm is expected to change in the near future due to the potential benefits of considering radiation-induced antitumor immunity during treatment planning. Towards this goal, we propose a minimal modeling framework based on key aspects of the tumor-immune system interplay to simulate the effects of radiation on tumors and the immunological consequences of radiotherapy. The impacts of tumor-associated vasculature and intratumoral oxygen-mediated heterogeneity on treatment outcomes are ininvestigated. The model provides estimates of the minimum radiation doses required for tumor eradication given a certain number of treatment fractions. Moreover, estimates of treatment duration for disease control given predetermined fractional radiation doses can be also obtained. Although theoretical in nature, this study motivates the development and establishment of immune-based decision-support tools in radiotherapy planning.



## Introduction

Radiotherapy (RT) is used in at least two-thirds of cancer patients at some point during their disease course, and contributes to about 40% of curative treatments (Atun et al., 2015; Thompson et al., 2018). However, tumor relapse after RT due to radioresistance of cancer cells is inevitable for many patients. Therapeutic strategies to overcome resistance have long been hindered due to the radiation dose to the tumor is limited by the tolerance of adjacent normal tissues. Although, several RT-drug combinations have been explored to target various tumor microenvironment components for radiosensitization, locoregional tumor recurrence remains an obstacle to cure (Barker et al., 2015). Increasing evidence also demonstrates the existence of cancer stem cells within some heterogeneous tumors, which represent a small but highly radioresistant cell subpopulation difficult to exterminate by RT (Schaue and McBride, 2015; Krause et al., 2017). Thus, resistance to radiation either intrinsically or acquired, is a plausible reason why current fractionation regimes with the only aim to maximize the direct killing of cancer cells sometimes fail to induce complete tumor eradication. This supports a paradigm shift in RT planning towards treatment plans that consider, and effectively exploit, the potential direct and indirect effects of radiation that cause harm to surviving, radioresistant cancer cells.

Recent evidence suggests that RT increases the immunogenicity of cancer cells and induce tumor-specific immune responses both in mouse models and in humans (Park et al., 2014; Schaue and McBride, 2015; Kono et al., 2013). It is currently known that RT influences each step of the cancer immunity cycle (Formenti and Demaria, 2009; Fridman et al., 2017), inducing a second wave of antitumor immune responses (Kaur and Asea, 2012; Golden et al., 2012). In particular, radiation induces dying tumor cells

* Corresponding author at: Department of Systems Immunology and Braunschweig Integrated Centre of Systems Biology, Helmholtz Centre for Infection Research, Braunschweig, Germany.
*E-mail addresses:* juancarlos.lopezalfonso@helmholtz-hzi.de (J.C.L. Alfonso), mmh@theoretical-biology.de (M. Meyer-Hermann).
[1] Both authors equally contributed to this work.

https://doi.org/10.1016/j.jtbi.2019.110099
0022-5193/

to express significantly more tumor-associated antigens on their surface and to release danger signals such as damage-associated molecular patterns, a process known as immunogenic cell death. This promotes the activation of professional antigen-presenting cells (APCs), which then migrate to draining lymph nodes (DLNs). Within DLNs, T-cell exposure to activated APCs results in the activation and priming of T-cells which enter in the bloodstream as tumor-specific T-cells and infiltrate into the tumor microenvironment. The ability of RT to induce not only local tumor-specific immune responses, but also systemic immune-mediated effects at distant sites away from the irradiated target, is an observed phenomenon referred as the abscopal effect Formenti and Demaria (2013). This suggests that the positive immunostimulatory effects of radiation might be co-responsible of locoregional tumor control in some patients, since surviving radioresistant cells can be eliminated by the immune system.

In addition to the immune system, a key microenvironmental factor influencing RT responses is the tumor-associated vasculature. Heterogeneity in cellular oxygenation within tumors, in particular the occurrence of hypoxia, is recognized as a cause of RT failure. This is associated to the fact that hypoxic cells are more radioresistant than normoxic cells due to reduced oxygen-mediated fixation of DNA damage (Moeller et al., 2007; Rockwell et al., 2009; Barker et al., 2015). This leads to the "blood vessel normalization hypothesis" which states that normalization of the dysfunctional tumor-associated vasculature can improve oxygenation and alleviate hypoxia for radiosensitization (Jain, 2005; 2014). Preclinical studies have also demonstrated that improved vascular functionality increases the infiltration of immune cells into the tumor bed and enhance their cytotoxic function (Hamzah et al., 2008; Schaaf et al., 2018). However, it is well-known that tumor vasculature plays an important role in sustaining tumor growth and facilitates relapse after therapy (Jain, 2005; Schaaf et al., 2018). Due to the opposing effects of vasculature on tumor dynamics, antitumor immune responses and radiosensitivity of cancer cells, tumor-associated vasculature is a key factor that should be accounted for during treatment planning.

Mathematical models incorporating different radiobiological and physical components has long been recognized as valuable decision-support tools in RT planning. Several models have been proposed to estimate the effect of radiation on cells (Fowler, 1989; O'Rourke et al., 2009; Sotolongo-Grau et al., 2010; McMahon, 2018), to determine tumor control and normal tissue complication probabilities (López Alfonso et al., 2018; Brodin et al., 2018; O'Rourke et al., 2009), to simulate growth of either homogeneous or heterogeneous tumors and predict their responses to different RT protocols (Enderling et al., 2009; Rockne et al., 2009; 2010; Enderling et al., 2010; Corwin et al., 2013; Kempf et al., 2013; Alfonso et al., 2014b; Kempf et al., 2015), and to optimize radiation dose distributions under clinical and technical constraints (Romeijn et al., 2006; Cappuccio et al., 2009; Alfonso et al., 2012; 2014a). On the other hand, several models considering the interactions between tumors and various immune cell subsets at different biological scales, and in some cases under the influence of microenvironmental factors such as cytokines and chemokines, have been also reported (Kuznetsov and Knott, 2001; Matzavinos et al., 2004; de Pillis et al., 2005; d'Onofrio, 2005; Eftimie et al., 2011; Hatzikirou et al., 2015). Recently, a mathematical model coupling local tumor-immune system dynamics and systemic T-cell trafficking in a metastatic setting has been proposed. This model considered radiation-induced immunity and it was used to simulate the evolution of tumor and immune cell populations in anatomically distant metastatic sites (abscopal effect) following surgical resection and RT (Poleszczuk et al., 2016; Poleszczuk and Enderling, 2018; Walker et al., 2018). In the same line, a different model suggested that radiation to the tumor bulk could induce a more robust immune response and better harness the synergy of RT and antitumor immunity than postsurgical radiation to the tumor bed (López Alfonso et al., 2019).

Herein, we present a modeling framework to simulate the effects of intratumoral oxygen-mediated heterogeneity and the immunological consequences of RT on tumor responses. With the aim of reducing the total number of model parameters, we implement a control engineering approach in the context of impulsive control theory, to propose a simplified version of the model that could be considered as a decision-support system for RT planning. This minimal framework allows to determine time-dose fractionation regimens that consider the RT effects on the tumor-immune system interplay.

## Materials and methods

### *A model of tumor-effector cell response to radiotherapy*

We further develop a previous model of tumor-effector cell interactions calibrated based on murine experiments of tumor growth (Hatzikirou et al., 2015; Reppas et al., 2016; Hatzikirou et al., 2017) to investigate the immunological consequences of RT. The proposed model is given by the following system of ordinary differential equations

$$\frac{dR}{dt} = \frac{1}{3}(\lambda_M B - \lambda_A)R + \lambda_M(1-B)L_D\left(\frac{1}{\tanh(R/L_D)} - \frac{L_D}{R}\right) - cER\frac{1}{R^{(1-B)}+1}, \tag{1}$$

$$\frac{dE}{dt} = r\frac{R^3}{K+R^3}E - \frac{d_1R^3}{R^{(1-B)}+1}E - d_0E + \sigma + \eta D^3, \quad t \neq \tau_i \tag{2}$$

$$\frac{dD}{dt} = -\theta D, \tag{3}$$

where $R(t)$ is the average tumor radius, $E(t)$ represents the concentration of effector cells in the tumor microenvironment and $D(t)$ is the fraction of tumor radius reduced by radiation which represents the fraction of irradiated cancer cells undergoing immunogenic cell death. The time coordinate $t$ has been omitted in Eqs. (1)–(3) for notation simplicity. Fig. 1A shows a schematic representation of the model given in Eqs. (1)–(3).

The first and second terms of Eq. (1) represent the vascular and avascular tumor growth respectively, where $B \in [0, 1]$ is a dimensionless parameter that represents the degree of functional tumor-associated vasculature, i.e. blood vessels that feed growing tumors with oxygen and nutrients. We assume that in the limit of avascular tumor growth ($B = 0$) tumor-effector cell interactions take place only at the tumor surface, while in fully vascularized tumors ($B = 1$) effector cells can potentially interact with any tumor cell. The parameters $\lambda_M$ and $\lambda_A$ are the mitotic and death rates of tumor cells, and $L_D$ is the intrinsic length scale resulting from nutrient dynamics, i.e. diffusion, supply and consumption. The last term of Eq. (1) models the killing of tumor cells by effectors at a rate $c$.

The first term of Eq. (2) models the recruitment of effector cells into the tumor microenvironment at a rate $r$, where $K$ is the tumor volume at which $r$ is half-maximal. We assume that without radiation, immune cells are recruited in response to signals released from both tumor cells and immunogenic dying cancer cells as a result of severe hypoxia and antitumor immune responses. The second and third terms of Eq. (2) represent the exhaustion of effector cells by their antitumor activity at a rate $d_1$ and spontaneous effector cell death at a rate $d_0$, respectively. Innate immunity $\sigma$ is represented as a baseline presence of effector cells at any time

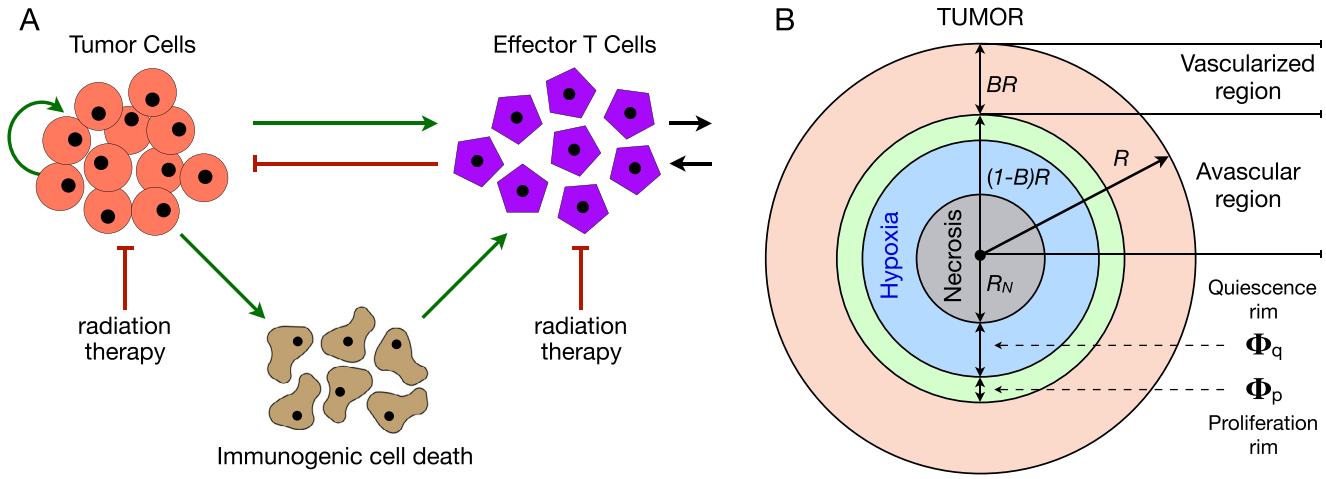


**Fig. 1. (A)** Schematic representation of the model given in Eqs. (1)–(3). Positive (green) and negative (red) feedbacks are represented. The arrows (black) pointing in and out to effector T cells represent the baseline recruitment of effector cells even in the absence of tumor cells and the natural death of effector cells, respectively. **(B)** A cross sectional view of an idealized spherical tumor of radius $R$ divided into an inner avascular region of radius $(1-B)R$ and an outer vascular layer of thickness $BR$. The inner avascular tumor region is composed by an outer proliferation rim of thickness $\Phi_p$ (green), an internal hypoxic layer of thickness $\Phi_q$ (blue) and a central necrotic core of radius $R_N$ (gray). (For interpretation of the references to color in this figure legend, the reader is referred to the web version of this article.)

(immunosurveillance), even in the absence of tumor cells. The last term of Eq. (2) models the recruitment of effector cells at a rate $\eta$, which is induced by the immunostimulatory signals from dying tumor cells that undergo immunogenic cell death as a consequence of RT. The strength of radiation-induced antitumor immune responses, characterized by subsequent infiltration of effector cells into the tumor bed, is assumed to depend on the fraction of lethally irradiated immunogenic tumor cells $D$. Eq. (3) describes the lysis of tumor cells sterilized by RT and the decrease of radiation-induced immunostimulatory signals at a rate $\theta$.

Simulations of the full model in Eqs. (1)–(3) were initialized with a small tumor radius of 0.1 mm, $0.13 \times 10^5$ effector cells (baseline presence) and no radiation-induced antitumor immunostimulation. These initial conditions result in tumors escaping immunosurveillance, and allow to then simulate the effect of RT. The sensitivity analysis of the model in Eqs. (1)–(3) without RT can be found in Hatzikirou et al. (2015), Reppas et al. (2016), where we provided phase portrait diagrams and performed the bifurcation analysis. In this study, we extended that model by considering the effects of RT, which only impacts the post-treatment system dynamics and do not affect the stability of the fixed points. Simulated tumors reaching a certain pre-defined size $R_0$ were treated with RT. Tumor diameters of 20 to 40 mm ($10 \leq R_0 \leq 20$ mm) where considered at time of treatment in agreement with reported sizes of colon cancer (tumor type for which the model was calibrated) at clinical presentation (Zlobec et al., 2010; Muralidhar et al., 2016). The delivery of each RT fraction and subsequent responses to radiation of both effector and tumor cells were assumed instantaneous, i.e. faster than the cell-cycle duration. Tab. 1 summarizes the parameter values used in model simulations. The mathematical model was implemented and simulated in Matlab, see www.mathworks.com.

*Modeling cell population responses to radiotherapy*

At each RT fraction of dose $d$ at time $t = \tau_i$, the radiation-induced change in the system variables $R$, $E$ and $D$ in Eqs. (1)-(3) are given by

$$\Delta R = -(BR + \Phi_p)(1 - S_p(d)) - \Phi_q(1 - S_q(d)), \tag{4}$$

$$\Delta E = -(1 - S_e(d))E, \qquad t = \tau_i \tag{5}$$

$$\Delta D = (BR + \Phi_p)(1 - S_p(d)) + \Phi_q(1 - S_q(d)), \tag{6}$$

where $\Delta x = x(\tau_i^+) - x(\tau_i)$ with $x = R, E, D$, and $\tau_i^+$ is the time instant after $\tau_i$.

The effect of radiation on tumor cells is simulated by means of the linear-quadratic (LQ) model Fowler (1989); McMahon (2018). According to it, the surviving fraction $S$ of cells receiving a radiation dose $d$ [Gy] is given by

$$S(d) = e^{-\xi(\alpha d + \beta d^2)}, \tag{7}$$

where $\alpha$ [$Gy^{-1}$] and $\beta$ [$Gy^{-2}$] are tumor-specific radiosensitivity parameters. As the model of tumor-effector cell interactions in Eqs. (1)–(3) was calibrated from in vivo experiments of murine CT26 (mouse colon carcinoma cell line) tumor growth (Hatzikirou et al., 2015), we consider $\alpha = 0.294$ $Gy^{-1}$ and $\beta = 0.0603$ $Gy^{-2}$ as estimated from 20 colon cancer cell lines (Leith et al., 1991). The parameter $\xi$ is incorporated in the LQ model to distinguish the different radiosensitivities of proliferative and quiescent (hypoxic) tumor cells (Enderling et al., 2009; Alfonso et al., 2014b). Accumulating evidence demonstrates that tumor cells exposed to hypoxia are about three-times more radioresistant than normoxic cycling cells (Rockwell et al., 2009; Moeller et al., 2007). We set $\xi = 1$ in $S_p$ and $\xi = 1/3$ in $S_q$ (Eq. (7)) to scale the radiosensitivity of proliferative and quiescent cancer cells, respectively (Enderling et al., 2009; Alfonso et al., 2014b). Thus, tumor radiosensitivity is determined by the intrinsic radiosensitivity of tumor cells ($\alpha$ and $\beta$ parameters of the LQ model) and modulated by microenvironmental conditions such as hypoxia (parameter $\xi$ in Eq. (7)).

At the time of irradiation, we consider tumors divided into an outer vascularized layer of thickness $BR$ and an inner avascular region of radius $(1-B)R$, see Fig. 1B. Additionally, the inner avascular region consists of a proliferation rim $\Phi_p$ determined by the diffusion of oxygen from the surrounding functional blood vessels in the outer vascularized tumor region, an intermediate quiescence region $\Phi_q$ in which tumor cells are hypoxic, and a central necrotic core of radius $R_N$. Accordingly, $(BR + \Phi_p)$ and $\Phi_q$ in Eq. (4) represent the proliferative and quiescent tumor regions, respectively. Experimental estimates of $\Phi_p = bR^{2/3}$ and $\Phi_q = aR^{2/3}$ have been previously used to model avascular tumor growth (see Table 1), where the two-thirds power law reflects a surface-to-volume ratio that can be biologically interpreted as oxygen diffusing through

**Table 1**
Parameter values used in model simulations.

| Parameter | Description | Value | Units | Source |
|---|---|---|---|---|
| $\lambda_M$ | Mitotic rate of tumor cells | 1.34 | days$^{-1}$ | Alessandri et al. (2013); Delarue et al. (2013) |
| $\lambda_A$ | Death rate of tumor cells | 0.14 | days$^{-1}$ | Hatzikirou et al. (2015) |
| $B$ | Degree of functional tumor vascularization | [0,1] | - | Hatzikirou et al. (2015) |
| $L_D$ | Characteristic nutrient diffusion length | 0.3 | mm | Cristini et al. (2008); Hatzikirou et al. (2015) |
| $c$ | Killing rate of tumor cells by effector cells | 0.03 | cells$^{-1}$ days$^{-1}$ | Hatzikirou et al. (2015) |
| $r$ | Recruitment rate of effector cells in response to tumor burden | 0.65 | days$^{-1}$ | Hatzikirou et al. (2015) |
| $K$ | Immune stimulation damping coefficient at which r is half-maximal | 2.72 | mm$^3$ | d'Onofrio (2005); Kuznetsov et al. (1994); de Pillis et al. (2005) |
| $d_0$ | Death rate of effector cells | 0.37 | days$^{-1}$ | Kuznetsov and Knott (2001); Su et al. (2009) |
| $d_1$ | Inactivation rate of effector cells by their antitumor activity | 0.01 | mm$^{-3}$ days$^{-1}$ | d'Onofrio (2005); Kuznetsov et al. (1994); de Pillis et al. (2005) |
| $\sigma$ | Baseline recruitment of effector cells | $0.13 \times 10^5$ | cells days$^{-1}$ | Kuznetsov et al. (1994) |
| $\eta$ | Radiation-induced effector cell recruitment rate | $7.5 \times 10^{-4}$ | cells mm$^{-3}$ days$^{-1}$ | *Estimated* |
| $\theta$ | Decay rate of immunostimulatory signals from irradiated tumor cells undergoing immunogenic cell death | 0.065 | days$^{-1}$ | *Estimated* |
| $a$ | Base necrotic thickness | 0.42 | mm$^{1/3}$ | Kansal et al. (2000); Schmitz et al. (2002) |
| $b$ | Base proliferative thickness | 0.11 | mm$^{1/3}$ | Kansal et al. (2000); Schmitz et al. (2002) |

the avascular tumor region surface (Kansal et al., 2000; Schmitz et al., 2002). In our model, we have that $\Phi_p = b((1-B)R)^{2/3}$ and $\Phi_q = a((1-B)R)^{2/3}$, where the lethal effect of a radiation dose $d$ on the proliferative and quiescent (hypoxic) tumor regions is given by $(BR+\Phi_p)\left(1-S_p(d)\right)$ and $\Phi_q\left(1-S_q(d)\right)$, see Eqs. (4) and (6).

The effect of radiation on tumor-infiltrating effector cells in Eq. (5) is considered based on experimental data of radiation-induced apoptosis in lymphocytes obtained from blood samples after exposure to acute doses of 2 to 8 Gy (Schnarr et al., 2007). Apoptosis is one of the dominant modes of cell killing induced by radiation in lymphocytes (Dewey et al., 1995), and correlation between the intensity of apoptosis in lymphocytes and radiation dose have been reported (Cui et al., 1999; Schnarr et al., 2007). The experimentally measured dose-response curve of effector cells was fitted to a two-term exponential function of the form $S_e(d) = \kappa_1 e^{-\rho_1 d} + \kappa_2 e^{-\rho_2 d}$, with $\kappa_1 = 0.29$, $\kappa_2 = 0.71$, $\rho_1 = 1.69$ Gy$^{-1}$ and $\rho_2 = 0.08$ Gy$^{-1}$. The expression $(1-S_e(d))$ represents the fraction of effector cells killed by a radiation dose $d$, see Eq. (5).

*Model linearization*

We linearize the model in Eqs. (1)–(6) around its desired equilibrium point $(R^*, E^*, D^*) = (0, \frac{\sigma}{d_0+1}, 0)$. The tumor size and the fraction of irradiated cancer cells undergoing immunogenic cell death are zero, and the concentration of effector cells in the tumor microenvironment is at the steady state point $\frac{\sigma}{d_0+1}$ (see Appendix A for further details). Linearization of system variables $E$ and $D$ leads to $dE/dt \equiv \dot{E} = -d_0(E-E^*)$ and $dD/dt \equiv \dot{D} = -\theta D$. Around $R^* = 0$, linearization of the $R$ dynamics with respect to $E$ is washed out leading to the following simplified model

$$\dot{R} = \frac{1}{3}(\lambda_M B - \lambda_A)R + \lambda_M(1-B)L_D\left(\frac{1}{\tanh(R/L_D)} - \frac{L_D}{R}\right) - \frac{c\sigma}{d_0+1}\frac{R}{R^{(1-B)}+1}, \quad t \neq \tau_i \tag{8}$$

$$\Delta R = -(BR+\Phi_p)(1-S_p(d)) - \Phi_q(1-S_q(d)), \tag{9}$$

Then, using the Taylor series we obtain

$$\dot{R} = \left(\frac{\lambda_M - \lambda_A}{3} - c\frac{\sigma}{d_0+1}\right)R + o(R^2) \tag{10}$$

as a linear approximation of the tumor radius $R$ dynamics (see Appendix A). The linear approximation of $\Delta R$ in Eq. (9) is given by

$$\Delta R = [-(B+\Phi_{p_0}(1-B))(1-S_p(d)) - \Phi_{q_0}(1-B)(1-S_q(d))]R \tag{11}$$

where

$$\Phi_{p_0} = \frac{b}{((1-B)R_0)^{1/3}}, \qquad \Phi_{q_0} = \frac{a}{((1-B)R_0)^{1/3}}, \tag{12}$$

and $R_0$ is the pre-treatment tumor radius. Supplemental Fig. A1 in Appendix A shows that this linear approximation of $\Delta R$ is accurate compared to the non-linear expression in Eq. (9).

Model linearization allows to significantly reduce the number of parameters resulting in a simpler model easier to interpret and parametrize. Simple models are always desired in both experimental and clinical settings for validation and potential use. The immune system dynamics are not considered in the linear model in Eqs. (10) and (11), but later included in order to accurately reproduce the full model predictions (Eq. (23)). Notice that linearization is part of the linear impulsive control theory used to linearize the proposed model Eq. (1)-(6), and it is not used for a classical linear stability analysis, but rather to devise a dose administration protocol into stabilizing the cancer-free state.

*Solution of the linear model*

The linear, reduced-order model in Eqs. (10) and (11) can be rewritten in a simplified form as

$$\dot{R} = AR, \qquad t \neq \tau_i \tag{13}$$

$$\Delta R = QR, \qquad t = \tau_i \tag{14}$$

where

$$A = \frac{\lambda_M - \lambda_A}{3} - c\frac{\sigma}{d_0+1}, \qquad t = \tau_i \tag{15}$$

$$Q = -(B+\Phi_{p_0}(1-B))(1-S_p(d)) - \Phi_{q_0}(1-B)(1-S_q(d)). \tag{16}$$

We assume fractionated RT protocols as a train of equidistant impulses separated by $\delta = \tau_{i+1} - \tau_i$, with treatment fractions

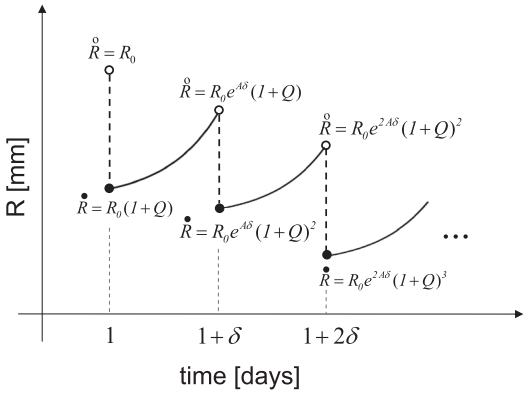


**Fig. 2.** Schematic representation of a tumor treated by fractionated radiotherapy as described by Eq. (19).

delivered at times $\tau_i$. Thus, $\delta$ represents a constant inter-fractional time. In this context, RT can be interpreted as a stabilization problem with the control objective of reducing $R$ to zero by using the linear control gain $Q$. Based on the stability theorem of linear impulsive control systems (Yang, 2001), the system in Eqs. (13) and (14) is stabilized (i.e. the point $R = 0$ becomes stable) if the following condition is satisfied

$$A + \frac{1}{\delta}\ln|1+Q| < 0. \tag{17}$$

Then, by substituting the expressions of $A$ and $Q$ in Eqs. (15) and (16) into the stabilizing condition in Eq. (17), and solving it with respect to $d$, we have that

$$d > d_s = \frac{-\alpha + \sqrt{\alpha^2 - 12\beta \ln C}}{2\beta}, \tag{18}$$

where $d_s$ is the minimum asymptotically stabilizing dose of the linear impulsive control system in Eqs. (13) and (14), and $C$ is a function depending on the degree of functional tumor-associated vasculature $B$, the tumor-immune system dynamic parameters in Eq. (15), the time between RT fractions $\delta$, and the size of the proliferative and hypoxic tumor regions, see Eq. (B7) in Appendix B for more details. Notice that $d_s$ does not only depend on the radiosensitivity parameters $\alpha$ and $\beta$ of the LQ model, but also on the pre-treatment tumor size $R_0$, functionality of tumor-associated vasculature $B$ and specific tumor and immune system parameters.

Beyond the asymptotic stability of the linear system in Eqs. (13) and (14), radiation doses $d > d_s$ for tumor eradication in a pre-defined number of treatment fractions, such as currently used for fractionated RT, need to be derived. For that purpose, we first solve the linear impulsive control system in Eqs. (13) and (14) for which the analytical solution is given by

$$R(t) = R_0\, e^{A(t-t_0)}\,(1+Q)^{N(t,t_0)}, \qquad t \geq t_0 \tag{19}$$

where $t_0$ is the time at which the first treatment fraction is applied and $N(t, t_0)$ is the number of RT fractions (impulses) delivered in the time interval $t_0$ to $t$. Fig. 2 shows a schematic representation of a tumor treated by fractionated RT as described by Eq. (19). We denote by $\overset{\circ}{R}$ and $\overset{\bullet}{R}$ the tumor size before and immediately after the delivery of each RT fraction. Based on Eq. (19), we have that $\overset{\circ}{R}$ and $\overset{\bullet}{R}$ at time $t = 1 + (j-1)\delta$, i.e. at the j-th treatment fraction, are given by

$$\overset{\circ}{R}(t = 1 + (j-1)\delta) = R_0\, e^{A(j-1)\delta}\,(1+Q)^{j-1}, \tag{20}$$

$$\overset{\bullet}{R}(t = 1 + (j-1)\delta) = R_0\, e^{A(j-1)\delta}\,(1+Q)^{j}, \tag{21}$$

where radiation-induced tumor control is assumed when the following condition is fulfilled

$$\overset{\bullet}{R} - R_N \leq l, \tag{22}$$

with $l << 1$ mm, and where $R_N = (1-B)\overset{\circ}{R} - \Phi_p - \Phi_q$ is the radius of the inner necrotic core with no viable tumor cells. We define by $t_E$ the time from the first treatment fraction delivery at which the condition in Eq. (22) is satisfied, i.e. the time of tumor eradication.

The analytical solution in Eq. (19) of the linear system given by Eqs. (13) and (14), together with the stop condition in Eq. (22), are used for two different treatment planning goals/objectives: (*i*) to determine the minimum fractional dose $d > d_s$ required for tumor eradication in a certain number of treatment fractions, or (*ii*) to estimate the overall treatment time, i.e. number of fractions, required for successful therapeutic outcomes given a pre-defined fractional dose $d > d_s$.

### *Incorporating antitumor immune responses into the linear model*

Tumor growth dynamic simulated with the linear model in Eqs. (13) and (14) are only limited by the baseline recruitment of effector cells. In particular, the death rate of tumor cells owing to effector cells $c$, baseline recruitment rate of effector cells $\sigma$ and natural death rate of effector cells $d_0$ are the only immune system-related parameters involved in the linear model formulation, see Eq. (15). We incorporate the antitumor immune system responses in the second term of Eq. (15) as follows

$$A = \frac{\lambda_M - \lambda_A}{3} - c\left(\frac{\sigma}{d_0+1} + \Theta_I(B)\right), \tag{23}$$

where $\Theta_I(B)$ is a linear function depending on $B$ that represents the amount of effector cells recruited to the tumor microenvironment in response to tumor burden and immunostimulatory effects of RT. Accumulating evidence supports that dysfunctional tumor vasculature (low values of $B$) is inhibitory to the extravasation of effector cells into the tumor bed and promotes a state of immunosuppression (Schmittnaegel and De Palma, 2017; Schaaf et al., 2018). However, functional reprogramming (increasing values of $B$), for instance by normalization or stress alleviation strategies (Jain, 2005; Stylianopoulos et al., 2012; Jain, 2014), improves effector cell trafficking into tumors and the efficacy of anticancer treatments (Schmittnaegel and De Palma, 2017). Accordingly, we assume that the amount of effector cells recruited to the tumor bed ($\Theta_I(B)$) depends on the functional degree of tumor-associated vascularity $B$. The biological consequences of effector cells are explored by considering key immune system-related parameters such as recruitment of immune cells, killing of tumor cells by effector cells, and inactivation/exhaustion of immune cells by their cytotoxic action against tumor cells. Moreover, the impact of immune cell killing by radiation and subsequent antitumor immune responses on tumor control are also investigated.

## Results

### *Performance analysis of the linear model without antitumor immune responses*

We first assess the linear model without antitumor immune responses in Eqs. (13) and (14) for reproducing the results of the full model in Eqs. (1)–(6). To that end, fractionated RT regimens at varying radiation doses $d$ are simulated with both models, and the number of treatment fractions required for tumor eradication are estimated. Fig. 3 shows the resulting treatment duration for tumor removal $t_E$ by considering RT fractions given once per day, i.e.

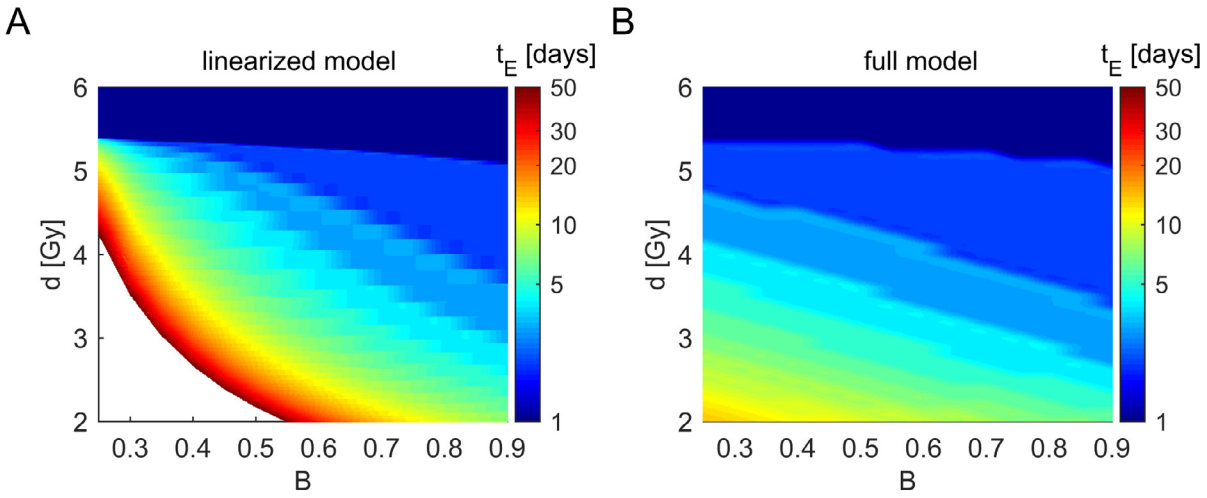


**Fig. 3.** Performance comparison of the (**A**) linear model without antitumor immune responses in Eqs. (13) and (14) with the (**B**) full model in Eqs. (1)–(6). Simulation maps show the time to tumor eradication $t_E$ with respect to radiation dose $d$ and degree of functional tumor-associated vasculature $B$. The white region in (A) corresponds to $t_E > 50$ days. RT fractions were delivered once per day. Simulations were obtained for a pre-treatment tumor size of $R_0 = 15$ mm, and the remaining parameter values are as in Table 1.

$\delta = 1$, and a pre-treatment tumor size of $R_0 = 15$ mm. Both models predict that more treatment fractions are required for tumor control with both decreasing radiation dose $d$ and degree of functional tumor-associated vasculature $B$. Model results suggest plausibility that vascular normalization could be used as a radiosensitizer therapeutic strategy to treat localized tumors when combined with RT.

For the simulated tumors in Fig. 3, which are characterized by different degrees of functional tumor-associated vasculature $B$, the linear model without antitumor immunity predicted tumor eradication after longer courses of RT (Fig. 3A) compared to the full model (Fig. 3B). The linear model results in $t_E$ between 1 and 50 days for the parameter ranges of $B$ and $d$ simulated, while $t_E$ ranges from 1 to 14 days in the full model. Fig. 3A shows that the

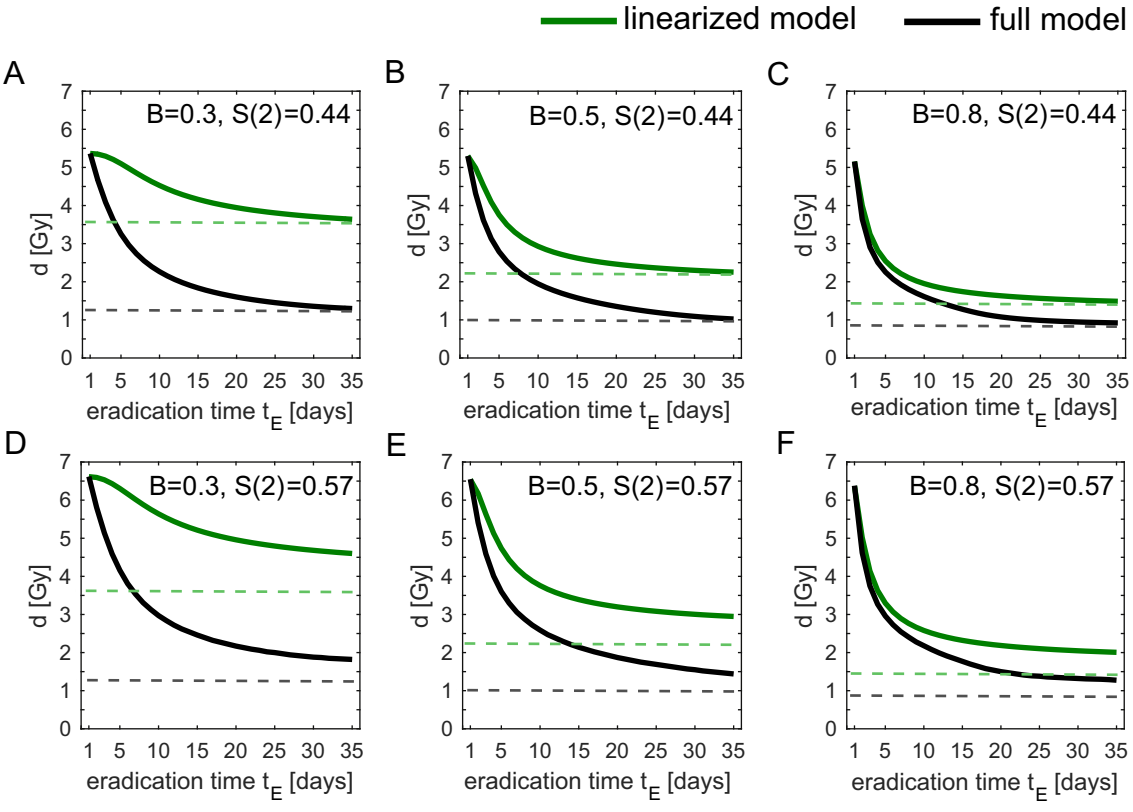


**Fig. 4.** Intrinsic tumor radiosensitivity and degree of functional vasculature $B$ effects on the minimal radiation dose ($d$) required for tumor eradication given the number of daily treatment fractions ($t_E$). Dose-time predictions of the (green) linear model in Eqs. (13) and (14) and (black) the full model in Eqs. (1)–(6) for different values of $B$ and surviving fraction of tumor cells at 2 Gy ($S(2)$, Eq. (7)). $S(2)$ is determined by the LQ model in Eq. (7) with (A-C) $\alpha = 0.294$ Gy$^{-1}$ and $\beta = 0.0603$ Gy$^{-2}$, and (D-F) $\alpha = 0.19$ Gy$^{-1}$ and $\beta = 0.044$ Gy$^{-2}$, which are in a range experimentally estimated for the tumor type considered (Leith et al., 1991). Simulations were obtained for a pre-treatment tumor size of $R_0 = 15$ mm, and the remaining parameter values are as in Tab. 1. (For interpretation of the references to color in this figure legend, the reader is referred to the web version of this article.)

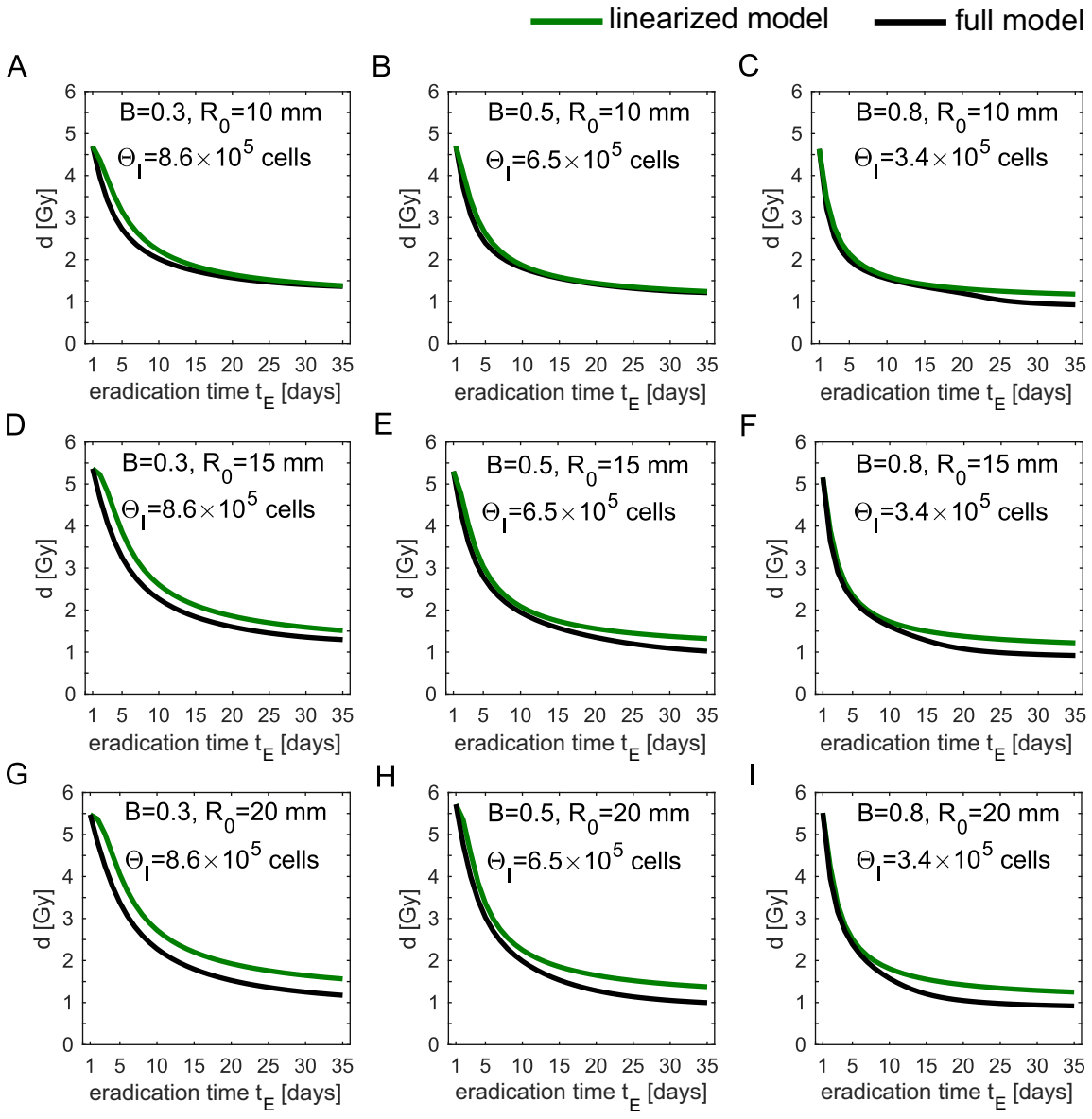


**Fig. 5.** Effects of the immune system-related parameter $\Theta_I$ (Eq. (23)) in the predictions of the linear model in Eqs. (13) and (14). Dose-time predictions of the (green) linear model and (black) full model in Eqs. (1)–(6) for different degrees of functional tumor-associated vasculature $B$ and pre-treatment tumor size $R_0$. For each simulated parameter combination, $\Theta_I$ values were calculated from the linear relationship $\Theta_I(B) = -10.5B + 11.8$. The remaining model parameters are as in Table 1. (For interpretation of the references to color in this figure legend, the reader is referred to the web version of this article.)

linear model estimates eradication of poorly-vascularized tumors with $B < 0.5$ and treated with fractional doses $d < 4$ Gy after long RT fractionated regimes, in some cases with $t_E > 50$ days. On the other hand, predictions of treatment duration from the linear model with higher fractional doses are close to those obtained with the full model. Moreover, Fig. 3 also shows that both models suggest similar time-dose fractionated RT regimens to control better vascularized tumors with $B \geq 0.5$. This suggests a critical role of antitumor immune responses in poorly-vascularized, and thus more radioresistant tumors, to kill the surviving cancer cells after treatment.

Fig. 4 shows the effect of intrinsic tumor radiosensitivity and the degree of functional vasculature $B$ on the predicted dose and number of treatment fractions for tumor eradication. We compare tumors characterized by different combinations of radiosensitivity parameter values $\alpha$ and $\beta$ of the LQ model in Eq. (7). This results in different dose-response curves of the LQ model, in which the surviving fraction of tumor cells at 2 Gy ($S(2)$, Eq. (7)) is a defined value on this curve often used to compare the radiation sensitivities of tumors. Comparing Fig. 4A–C to Fig. 4D–F reveals that lower radiation doses are required to control well-vascularized tumors compared to poorly vascularized tumors. Moreover, modeling results also show that smaller increments on the radiation doses are required to control more intrinsically radioresistant tumors as the degree of functional tumor-associated vasculature increases. We notice that depending on tumor cell radiosensitivity and vascularity the full model reproduces fractional doses routinely used in conventionally fractionated RT, around 1.8 Gy day$^{-1}$ (Glimelius, 2013).

### *Considering antitumor immunity improves linear model predictions*

In the linear model in Eqs. (13) and (14) tumor growth dynamic and RT responses are not influenced by antitumor immune system responses. As a result, treatment regimens for tumor eradication resulting from the linear model represent an overestimation

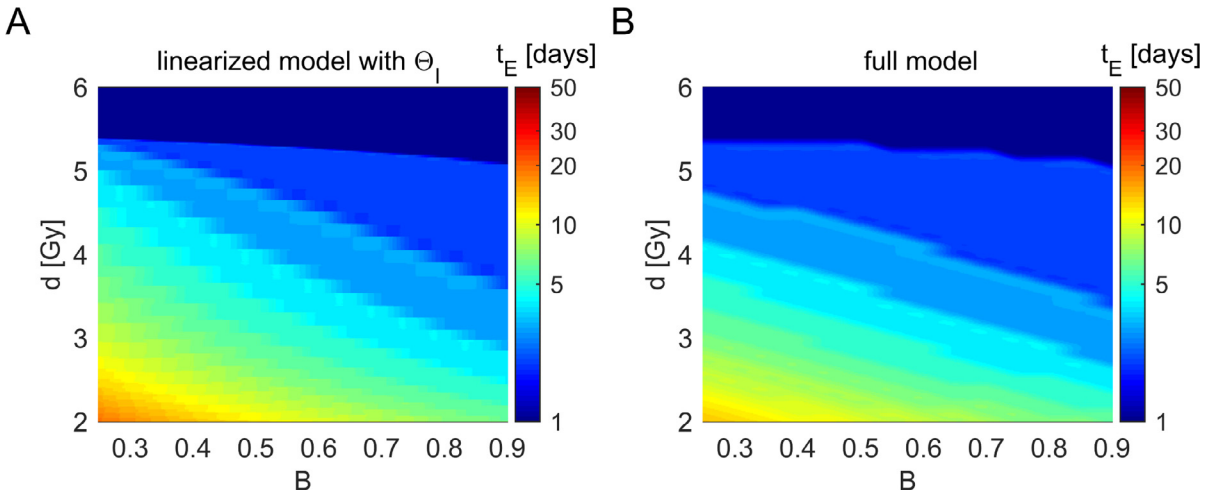


**Fig. 6.** Performance comparison of the (**A**) linear model in Eqs. (13) and (14) considering antitumor immune responses given by Eq. (23) with the (**B**) full model in Eqs. (1)–(6). Simulation maps show the time to tumor eradication $t_E$ with respect to fractional radiation doses $d$ and degrees of functional tumor-associated vasculature $B$. The linear relationship $\Theta_I(B) = -10.5B + 11.8$ was used to calculate the values of $\Theta_I$ in the modified linear model. Simulations were obtained for a pre-treatment tumor size of $R_0 = 15$ mm, and the remaining model parameters are as in Table 1.

of the predictions from the full model in Eqs. (1)–(6) as shown in Figs. 3 and 4. Fig. 4 shows that differences in the time-dose treatment predictions between the linear and full models strongly depend on the degree of functional tumor-associated vasculature $B$, with larger discrepancies in the case of poorly vascularized tumors. These differences can be compensated by considering the antitumor effects of the immune system as a linear function ($\Theta_I(B)$), which represents the amount of effector cells in the tumor microenvironment as a consequence of tumor presence and immunostimulatory effects of RT, see Eq. (23). Although, antitumor immune responses also depends on the pre-treatment tumor size $R_0$, model simulations evidence that they are more affected by $B$. Thus, we considered $\Theta_I$ as a function of $B$. For each simulated parameter combination in Fig. 5, the optimal $\Theta_I$ value minimizing the differences in time-dose treatment predictions between the linear and full models are calculated. We found that $\Theta_I$ accurately correlates with $B$ through a linear relationship $\Theta_I(B) = -10.5B + 11.8$ for the baseline parameter values in Table 1. Fig. 5 shows that time-dose predictions of the linear model taking into account $\Theta_I(B)$ accurately reproduce the full model results. Fig. 6 shows that $t_E$ now ranges from 1 and 19 days in the corrected linear model, while full model predictions of $t_E$ varies between 1 to 14 days. We highlight that both radiation doses and number of fractions for tumor control in Figs. 5 and 6 are in the ranges routinely used in clinical practice (Formenti and Demaria, 2009; Barker et al., 2015; Schaue and McBride, 2015).

*Impact of immune-related model parameters on $\Theta_I$(B)*

We now explore how the linear function $\Theta_I(B)$ in Eq. (23) depends on two key immune system-related model parameters; the killing rate of tumor cells by effector cells ($c$) and the radiation-induced effector cell recruitment rate ($\eta$). To that end, we consider 50% change in the baseline value of $c = 0.03$ cells$^{-1}$ days$^{-1}$ and different order of magnitudes for the baseline value of $\eta = 7.5 \times 10^{-4}$ cells mm$^{-3}$ days$^{-1}$, see Table 1 and Fig. 7. For the different value combinations of $c$, $\eta$ and $B$ simulated, we estimated the values of $\Theta_I(B)$ that minimize the differences on the time-dose treatment predictions between the linear and full models as done in Fig. 5. Fig. 7 shows that there exists a linear relationship between $\Theta_I$ and $B$ for all considered parameter sets. Moreover, $\Theta_I$ increases with lower values of $B$ irrespective of $c$, which evidences a critical role of antitumor immune responses for the eradication of radioresistant, poorly-vascularized tumors. Fig. 7 also shows that higher values of $\Theta_I(B)$ are required in the linear model to compensate the effect of stronger radiation-induced antitumor immune responses, i.e. by increasing $\eta$, in the full model. On the other hand, lower values of $\Theta_I(B)$ are required as $c$ increases due to a more efficient killing of tumor cells by effector cells. We notice that $\Theta_I(B)$ in Fig. 7B, which is determined by the baseline parameter values $c = 0.03$ cells$^{-1}$ days$^{-1}$ and $\eta = 7.5 \times 10^{-4}$ cells mm$^{-3}$ days$^{-1}$, corresponds to the case shown in Fig. 5.

*A minimal modeling framework for immune-based planning of radiotherapy*

The linear model in Eqs. (13) and (14) coupled with the linear function ($\Theta_I(B)$) in Eq. (23) has been demonstrated to accurately reproduce time-dose treatment predictions for tumor control of the full model in Eqs. (1)–(6). Tumor growth between treatment fractions simulated with the linear model is given by $\dot{R} = (T_G - I_E)R$, where $T_G = \frac{\lambda_M - \lambda_A}{3}$ is the net tumor growth, $I_E = c\left(\frac{\sigma}{d_0+1} + \Theta_I(B)\right)$ represents the antitumor immune responses, and $\Delta R = QR$ models the effect of radiation on the tumor, see Eqs. (13) and (14), (16) and (23). Upon an adequate parameter calibration and validation, the resulting linear model could be used as a minimal modeling framework ($i$) to determine the minimum fractional dose required for tumor eradication given the number of treatment fractions, or ($ii$) to estimate the treatment duration for cure given a fractional dose, see Fig. 8.

An appropriate tumor profiling, for instance, via tissue biopsy and/or medical imaging techniques is crucial for the use of decision-support modeling frameworks in RT planning. Image modalities, such as computed tomography (CT), magnetic resonance (MR) imaging and positron emission tomography (PET), provide useful anatomical and functional information of tumors (Pereira et al., 2014). In particular, clinical imaging allows to determine the pre-treatment tumor size, estimate metabolic activity and the degree of functional tumor-associated vasculature, as well as to estimate proliferation and dispersal rates (Baldock et al., 2014). Moreover, histopathological analysis of tissue samples obtained by biopsies before treatment could be used to assess the tumor-immune ecosystem composition (Hendry et al., 2017), de-

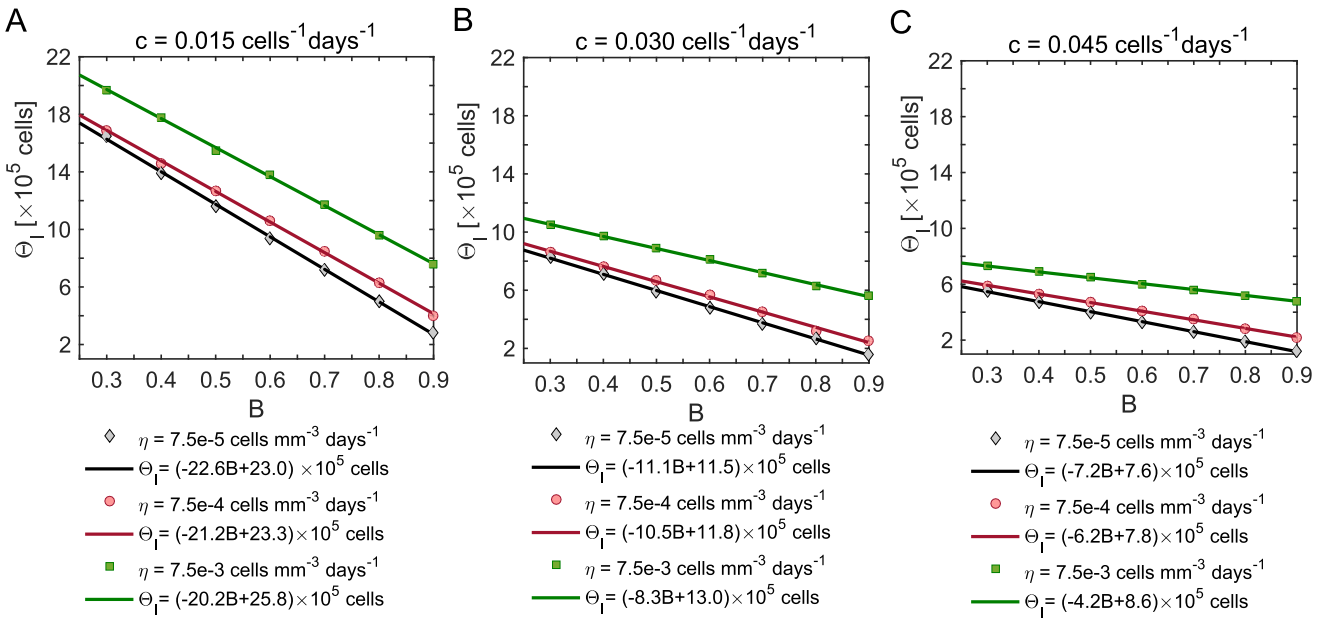


**Fig. 7.** Dependence of the linear function $\Theta_I(B)$ in Eq. (23) on the killing rate of tumor cells by effectors $c$ and the strength of radiation-induced immunostimulation $\eta$. Simulations were performed for $t_E$ varying between 1 to 35 days and a pre-treatment tumor size of $R_0 = 15$ mm. The remaining model parameters are as in Table 1.

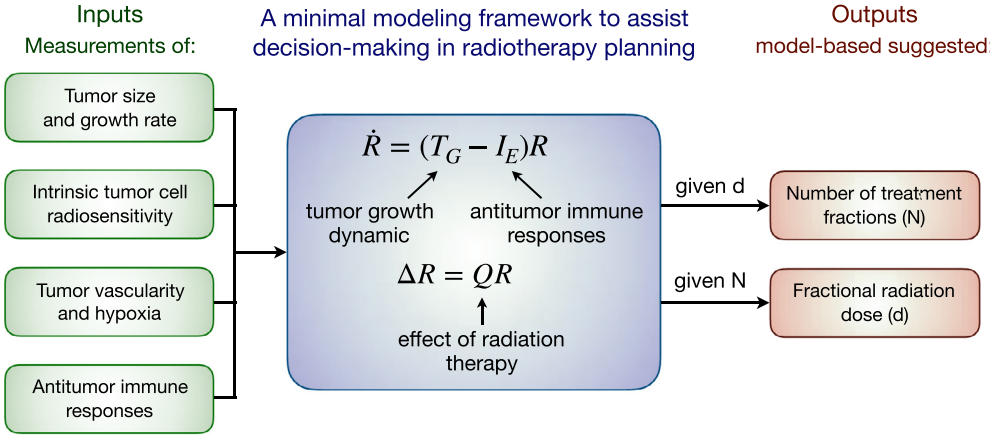


**Fig. 8.** Workflow to assist radiotherapy planning using the proposed simplified modeling framework. The green boxes at the left represent the (input) data that should be measured / estimated to parametrize the modeling framework in the central blue box, which then suggests (outputs, red boxes at the right) the number of treatment fractions $N$ required for tumor control given a fractional dose (d) or vice versa. (For interpretation of the references to color in this figure legend, the reader is referred to the web version of this article.)

termine the extent of tumor vascularity and hypoxia, and estimate the net proliferation rate of tumor cells (Macklin et al., 2012). The radiation effects on systemic antitumor immunity and estimates of recruitment rate of tumour-infiltrating immune cells could be derived from regular measurements of changes in populations of circulating immune cells during treatment (Sridharan et al., 2016).

The proposed modeling framework not only could assist decision making for individualized immune-based planning of RT when administered alone, but also in combination with other treatments such as chemotherapy or immunotherapy by tuning appropriate model parameters. Modeling results suggest that vasculature normalization, i.e. by increasing the model parameter $B$, is a plausible therapeutic strategy to enhance immune cell infiltration into the tumor bed and to reduce hypoxia-mediated radioresistance of tumor cells. In addition, combination of RT with a general form of immunotherapy that affects the efficacy of antitumor immune system responses, i.e. by modulating the killing rate of tumor cells by effectors $c$, could be also implemented.

## Discussion

Rapidly emerging evidence that radiation enhances both local and systemic antitumor immunity motivate a profound change in the manner we clinically prescribe radiotherapy (RT) (Formenti and Demaria, 2009; Golden et al., 2012; Kaur and Asea, 2012; Formenti and Demaria, 2013; Park et al., 2014). Although the potential therapeutic value of considering the synergy between radiation and the immune system during treatment planning is apparent, current practice still does not consider it. The proposed modeling framework intends to contribute towards establishing immune-based decision-support tools in RT planning. The goal in this study was to propose a simple model with as few parameters as possible, but still taking into account the main factors influencing tumor responses to RT. This model has the minimal required ingredients to simulate the immunological consequences of radiation. Such a simple model with potentially measurable parameters is needed in order to make it suitable for clinical applications. This

level of simplicity is necessary and can be sufficient to get reliable clinical predictions (Enderling et al., 2019).

Herein, we present a tumor-immune system interplay model previously calibrated on mouse data of tumor growth to simulate the immunological consequences of RT. The effects of tumor-associated vasculature on tumor growth dynamic- and antitumor immune responses, as well as the impact of intratumoral oxygen-mediated heterogeneity on treatment responses were considered. We then implemented a control engineering approach, in the context of impulsive control theory, to propose a simplified version of the full model as a decision-support system for immune-based RT planning. The resulting modeling framework designed to support decision-making in RT has a significantly reduced number of parameters which makes it easier to work with and parametrize, which is always desired in both experimental and clinical settings for validation and use. This framework allows to simulate tumor changes between treatment fractions which are determined by a balance between net tumor growth and antitumor immune responses. Simulations demonstrated that the proposed simplified model is able to reproduce the results of the full model while involving a reduced number of parameters. We described how this minimal modeling framework can be used to determine time-dose fractionation regimens for tumor control by considering the effects of radiation on the tumor-immune system interplay. Moreover, we also explored the impact on model predictions of relevant parameters that may represent the patient-specific biology of individual patients, including tumor vascularity and extend of hypoxia, strength of radiation-induced immune responses or pre-treatment tumor size. Although involving few parameters, the proposed modeling framework to assist decision-making in RT planning needs to be rigorously calibrated on human data and adequately validated. In particular, the effects of treatment parameters such as fractional dose and treatment duration, inter-tumor and inter-patient heterogeneity on induced antitumor immune responses need to be carefully estimated for the potential use of the proposed decision-support tool. Moreover, approaches to discern and assess the contribution of tumor-associated vasculature to antitumor immunity and radiation responses are required.

While considering the immunostimulatory potential of radiation during treatment planning is promising, there are still many challenges ahead (Formenti and Demaria, 2009; Kaur and Asea, 2012; Formenti and Demaria, 2013). A further understanding of the effects of radiation on the tumor microenvironment and underlying immunological processes that regulate both pro- and antitumor immunity, is urgently needed. Similarly, the precise impact of treatment planning variables such as fractional dose, treatment duration and frequency of RT on the tumor-immune ecosystem composition and subsequent immune responses remains unclear. Moreover, future efforts are also required to elucidate the radiobiological mechanisms and factors that might be responsible for, and potentially induce, the observed off-target immune-mediated antitumor effects of RT (abscopal effect) (Formenti and Demaria, 2013). We believe, however, that progress towards establishing RT protocols considering the immunological consequences of radiation would be facilitated by modeling frameworks, which provide a valuable ground for investigating tumor-immune cell interactions and evaluate different RT treatment plans. This exploratory study provides rationale and motivation for prospective evaluation of the immunogenicity of radiotherapy and continues paving the road for the translation of predictive modeling frameworks into clinical research as decision-support tools.

## Declaration of Competing Interest

The authors declare that no competing financial interests exist.

## CRediT authorship contribution statement

**Ghazal Montaseri:** Methodology, Formal analysis, Writing - original draft. **Juan Carlos López Alfonso:** Visualization, Formal analysis, Writing - original draft. **Haralampos Hatzikirou:** Visualization, Formal analysis, Supervision, Writing - original draft. **Michael Meyer-Hermann:** Supervision, Writing - original draft.

## Acknowledgments

JCLA, HH and MMH gratefully acknowledge the funding support of the Helmholtz Association of German Research Centers - Initiative and Networking Fund for the project on Reduced Complexity Models (ZT-I-0010). GM, JCLA, HH and MMH are also supported by the Systems Medicine project SYSIMIT (01ZX1308D) of the Federal Ministry of Education and Research (BMBF). MMH is additionally supported by the BMBF project Sys-Stomach (01ZX1310C), and the iMed – the Helmholtz Initiative on Personalized Medicine. HH is also funded by the BMBF projects MicMode-I2T (01ZX1710B) and MulticellML (01ZX1707C), as well as by the project SYSMIFTA (031L0085B) of the ERACOSYSMED initiative.

## Supplementary material

Supplementary material associated with this article can be found, in the online version, at 10.1016/j.jtbi.2019.110099.

## References

Alessandri, K., Sarangi, B.R., Gurchenkov, V.V., Sinha, B., Kießling, T.R., Fetler, L., Rico, F., Scheuring, S., Lamaze, C., Simon, A., Geraldo, S., Vignjevic, D., Doméjean, H., Rolland, L., Funfak, A., Bibette, J., Bremond, N., Nassoy, P., 2013. Cellular capsules as a tool for multicellular spheroid production and for investigating the mechanics of tumor progression in vitro. Proc. Natl. Acad. Sci. USA 110 (37), 14843–14848.

Alfonso, J., Buttazzo, G., García-Archilla, B., Herrero, M.A., Núñez, L., 2014. Selecting radiotherapy dose distributions by means of constrained optimization problems. Bull. Math. Biol. 76 (5), 1017–1044.

Alfonso, J.C.L., Jagiella, N., Núñez, L., Herrero, M.A., Drasdo, D., 2014. Estimating dose painting effects in radiotherapy: a mathematical model. PloS One 9 (2), e89380.

Alfonso, L., Carlos, J., Buttazzo, G., García-Archilla, B., Herrero, M.A., Núñez, L., 2012. A class of optimization problems in radiotherapy dosimetry planning. Discre. Contin. Dyn. Syst. Ser. B 17 (6).

Atun, R., Jaffray, D.A., Barton, M.B., Bray, F., Baumann, M., Vikram, B., Hanna, T.P., Knaul, F.M., Lievens, Y., Lui, T.Y.M., et al., 2015. Expanding global access to radiotherapy. Lancet Oncol. 16 (10), 1153–1186.

Baldock, A.L., Yagle, K., Born, D.E., Ahn, S., Trister, A.D., Neal, M., Johnston, S.K., Bridge, C.A., Basanta, D., Scott, J., et al., 2014. Invasion and proliferation kinetics in enhancing gliomas predict IDH1 mutation status. Neuro-oncology 16 (6), 779–786.

Barker, H.E., Paget, J.T.E., Khan, A.A., Harrington, K.J., 2015. The tumour microenvironment after radiotherapy: mechanisms of resistance and recurrence. Nat. Rev. Cancer 15 (7), 409.

Brodin, N.P., Kabarriti, R., Garg, M.K., Guha, C., Tomé, W.A., 2018. Systematic review of normal tissue complication models relevant to standard fractionation radiation therapy of the head and neck region published after the QUANTEC reports. Int. J. Radiat. Oncol. Biol. Phys. 100 (2), 391–407.

Cappuccio, A., Herrero, M.A., Nuñez, L., 2009. Biological optimization of tumor radiosurgery. Med. Phys. 36 (1), 98–104.

Corwin, D., Holdsworth, C., Rockne, R.C., Trister, A.D., Mrugala, M.M., Rockhill, J.K., Stewart, R.D., Phillips, M., Swanson, K.R., 2013. Toward patient-specific, biologically optimized radiation therapy plans for the treatment of glioblastoma. PloS One 8 (11), e79115.

Cristini, V., Frieboes, H.B., Li, X., Lowengrub, J.S., Macklin, P., Sanga, S., Wise, S.M., Zheng, X., 2008. Nonlinear modeling and simulation of tumor growth. In: Selected Topics in Cancer Modeling. Springer, pp. 1–69.

Cui, Y.F., Gao, Y.B., Yang, H., Xiong, C.Q., Xia, G.W., Wang, D.W., 1999. Apoptosis of circulating lymphocytes induced by whole body gamma-irradiation and its mechanism. J. Environ. Pathol. Toxicol. Oncol. Off. Organ Int. Soc. Environ. Toxicol. Cancer 18 (3), 185–189.

Delarue, M., Montel, F., Caen, O., Elgeti, J., Siaugue, J.M., Vignjevic, D., Prost, J., Joanny, J.F., Cappello, G., 2013. Mechanical control of cell flow in multicellular spheroids. Phys. Rev. Lett. 110 (13), 138103.

Dewey, W.C., Ling, C.C., Meyn, R.E., 1995. Radiation-induced apoptosis: relevance to radiotherapy. Int. J. Radiat. Oncol. Biol. Phys. 33 (4), 781–796.

d'Onofrio, A., 2005. A general framework for modeling tumor-immune system competition and immunotherapy: mathematical analysis and biomedical inferences. Phys. D Nonlinear Phenomena 208 (3), 220–235.

Eftimie, R., Bramson, J.L., Earn, D.J.D., 2011. Interactions between the immune system and cancer: a brief review of non-spatial mathematical models. Bull. Math. Biol. 73 (1), 2–32.

Enderling, H., Alfonso, J.C.L., Moros, E., Caudell, J.J., Harrison, L.B., 2019. Integrating mathematical modeling into the roadmap for personalized adaptive radiation therapy. Trends Cancer 5 (8), 467–474.

Enderling, H., Chaplain, M.A.J., Hahnfeldt, P., 2010. Quantitative modeling of tumor dynamics and radiotherapy. Acta Biotheor. 58 (4), 341–353.

Enderling, H., Park, D., Hlatky, L., Hahnfeldt, P., 2009. The importance of spatial distribution of stemness and proliferation state in determining tumor radioresponse. Math. Model. Nat. Phenom. 4 (3), 117–133.

Formenti, S.C., Demaria, S., 2009. Systemic effects of local radiotherapy. Lancet Oncol. 10 (7), 718–726.

Formenti, S.C., Demaria, S., 2013. Combining radiotherapy and cancer immunotherapy: a paradigm shift. JNCI J. Natl. Cancer Inst. 105 (4), 256–265.

Fowler, J.F., 1989. The linear-quadratic formula and progress in fractionated radiotherapy. Br. J. Radiol. 62 (740), 679–694.

Fridman, W.H., Zitvogel, L., Sautès-Fridman, C., Kroemer, G., 2017. The immune contexture in cancer prognosis and treatment. Nat. Rev. Clin. Oncol. 14 (12), 717.

Glimelius, B., 2013. Neo-adjuvant radiotherapy in rectal cancer. World J. Gastroenterol. WJG 19 (46), 8489.

Golden, E., Pellicciotta, I., Demaria, S., Barcellos-Hoff, M.H., Formenti, S.C., 2012. The convergence of radiation and immunogenic cell death signaling pathways. Front. Oncol. 2, 88.

Hamzah, J., Jugold, M., Kiessling, F., Rigby, P., Manzur, M., Marti, H.H., Rabie, T., Kaden, S., Gröne, H.-J., Hämmerling, G.J., et al., 2008. Vascular normalization in rgs5-deficient tumours promotes immune destruction. Nature 453 (7193), 410.

Hatzikirou, H., Alfonso, J., Mühle, S., Stern, C., Weiss, S., Meyer-Hermann, M., 2015. Cancer therapeutic potential of combinatorial immuno-and vasomodulatory interventions. J. R. Soc. Interface 12 (112), 20150439.

Hatzikirou, H., Alfonso, J.C.L., Leschner, S., Weiss, S., Meyer-Hermann, M., 2017. Therapeutic potential of bacteria against solid tumors. Cancer Res. 77 (7) 1553–63.

Hendry, S., Salgado, R., Gevaert, T., Russell, P.A., John, T., Thapa, B., Christie, M., Estrada, M.V., Gonzalez-Ericsson, P.I., Sanders, M., et al., 2017. Assessing tumor-infiltrating lymphocytes in solid tumors: a practical review for pathologists and proposal for a standardized method from the international immunooncology biomarkers working group: part 1: assessing the host immune response, TILs in invasive breast carcinoma and ductal carcinoma in situ, metastatic tumor deposits and areas for further research. Adv. Anat. Pathol. 24 (5), 235–251.

Jain, R.K., 2005. Normalization of tumor vasculature: an emerging concept in antiangiogenic therapy. Science 307 (5706), 58–62.

Jain, R.K., 2014. Antiangiogenesis strategies revisited: from starving tumors to alleviating hypoxia. Cancer Cell 26 (5), 605–622.

Kansal, A.R., Torquato, S., Harsh, G.R., Chiocca, E.A., Deisboeck, T.S., 2000. Simulated brain tumor growth dynamics using a three-dimensional cellular automaton. J. Theor. Biol. 203 (4), 367–382.

Kaur, P., Asea, A., 2012. Radiation-induced effects and the immune system in cancer. Front. Oncol. 2, 191.

Kempf, H., Bleicher, M., Meyer-Hermann, M., 2015. Spatio-temporal dynamics of hypoxia during radiotherapy. PLoS One 10 (8), e0133357.

Kempf, H., Hatzikirou, H., Bleicher, M., Meyer-Hermann, M., 2013. In silico analysis of cell cycle synchronisation effects in radiotherapy of tumour spheroids. PLoS Comput. Biol. 9 (11), e1003295.

Kono, K., Mimura, K., Kiessling, R., 2013. Immunogenic tumor cell death induced by chemoradiotherapy: molecular mechanisms and a clinical translation. Cell Death Dis. 4 (6), e688.

Krause, M., Dubrovska, A., Linge, A., Baumann, M., 2017. Cancer stem cells: radioresistance, prediction of radiotherapy outcome and specific targets for combined treatments. Adv. Drug Deliv. Rev. 109, 63–73.

Kuznetsov, V., Makalkin, I., Taylor, M., Perelson, A., 1994. Nonlinear dynamics of immunogenic tumors: parameter estimation and global bifurcation analysis. Bull. Math. Biol. 56 (2), 295–321. doi:10.1016/S0092-8240(05)80260-5.

Kuznetsov, V.A., Knott, G.D., 2001. Modeling tumor regrowth and immunotherapy. Math. Comput. Model. 33 (12–13), 1275–1287.

Leith, J.T., Padfield, G., Faulkner, L.E., Quinn, P., Michelson, S., 1991. Effects of feeder cells on the x-ray sensitivity of human colon cancer cells. Radiother. Oncol. 21 (1), 53–59.

López Alfonso, J.C., Parsai, S., Joshi, N., Godley, A., Shah, C., Koyfman, S.A., Caudell, J.J., Fuller, C.D., Enderling, H., Scott, J.G., 2018. Temporally-feathered intensity modulated radiation therapy: a technique to reduce normal tissue toxicity. Medical physics 45 (7), 3466–3474.

López Alfonso, J.C., Poleszczuk, J., Walker, R., Kim, S., Pilon-Thomas, S., Conejo-Garcia, J.J., Soliman, H., Czerniecki, B., Harrison, L.B., Enderling, H., 2019. Immunologic consequences of sequencing cancer radiotherapy and surgery. JCO Clin. Cancer Inform. 3, 1–16.

Macklin, P., Edgerton, M.E., Thompson, A.M., Cristini, V., 2012. Patient-calibrated agent-based modelling of ductal carcinoma in situ (DCIS): from microscopic measurements to macroscopic predictions of clinical progression. J. Theor. Biol. 301, 122–140.

Matzavinos, A., Chaplain, M.A.J., Kuznetsov, V.A., 2004. Mathematical modelling of the spatio-temporal response of cytotoxic t-lymphocytes to a solid tumour. Math. Med. Biol. 21 (1), 1–34.

McMahon, S.J., 2018. The linear quadratic model: usage, interpretation and challenges. Phys. Med. Biol. 64 (1), 01TR01.

Moeller, B.J., Richardson, R.A., Dewhirst, M.W., 2007. Hypoxia and radiotherapy: opportunities for improved outcomes in cancer treatment. Cancer Metastasis Rev. 26 (2), 241–248.

Muralidhar, V., Nipp, R.D., Ryan, D.P., Hong, T.S., Nguyen, P.L., Wo, J.Y., 2016. Association between very small tumor size and increased cancer-specific mortality in node-positive colon cancer. Dis. Colon Rectum 59 (3), 187–193.

O'Rourke, S., McAneney, H., Hillen, T., 2009. Linear quadratic and tumour control probability modelling in external beam radiotherapy. J. Math. Biol. 58 (4–5), 799.

Park, B., Yee, C., Lee, K.-M., 2014. The effect of radiation on the immune response to cancers. Int. J. Mol. Sci. 15 (1), 927–943.

Pereira, G.C., Traughber, M., Muzic, R.F., 2014. The role of imaging in radiation therapy planning: past, present, and future. BioMed Res. Int. 2014, 231090. https://www.ncbi.nlm.nih.gov/pmc/articles/PMC4000658/

de Pillis, L.G., Radunskaya, A.E., Wiseman, C.L., 2005. A validated mathematical model of cell-mediated immune response to tumor growth. Cancer Res. 65 (17), 7950–7958.

Poleszczuk, J., Enderling, H., 2018. The optimal radiation dose to induce robust systemic anti-tumor immunity. Int. J. Mol. Sci. 19 (11), 3377.

Poleszczuk, J.T., Luddy, K.A., Prokopiou, S., Robertson-Tessi, M., Moros, E.G., Fishman, M., Djeu, J.Y., Finkelstein, S.E., Enderling, H., 2016. Abscopal benefits of localized radiotherapy depend on activated t-cell trafficking and distribution between metastatic lesions. Cancer Res..

Reppas, A.I., Alfonso, J., Hatzikirou, H., 2016. In silico tumor control induced via alternating immunostimulating and immunosuppressive phases. Virulence 7 (2). 174–86

Rockne, R., Alvord, E.C., Rockhill, J.K., Swanson, K.R., 2009. A mathematical model for brain tumor response to radiation therapy. J. Math. Biol. 58 (4–5), 561.

Rockne, R., Rockhill, J.K., Mrugala, M., Spence, A.M., Kalet, I., Hendrickson, K., Lai, A., Cloughesy, T., AlvordJr, E.C., Swanson, K.R., 2010. Predicting the efficacy of radiotherapy in individual glioblastoma patients in vivo: a mathematical modeling approach. Phys. Med. Biol. 55 (12), 3271.

Rockwell, S., Dobrucki, I.T., Kim, E.Y., Marrison, S.T., Vu, V.T., 2009. Hypoxia and radiation therapy: past history, ongoing research, and future promise. Curr. Mol. Med. 9 (4), 442–458.

Romeijn, H.E., Ahuja, R.K., Dempsey, J.F., Kumar, A., 2006. A new linear programming approach to radiation therapy treatment planning problems. Oper. Res. 54 (2), 201–216.

Schaaf, M.B., Garg, A.D., Agostinis, P., 2018. Defining the role of the tumor vasculature in antitumor immunity and immunotherapy. Cell Death Dis. 9 (2), 115.

Schaue, D., McBride, W.H., 2015. Opportunities and challenges of radiotherapy for treating cancer. Nat. Rev. Clinical oncology 12 (9), 527.

Schmittnaegel, M., De Palma, M., 2017. Reprogramming tumor blood vessels for enhancing immunotherapy. Trends Cancer 3 (12), 809–812.

Schmitz, J.E., Kansal, A.R., Torquato, S., 2002. A cellular automaton model of brain tumor treatment and resistance. Comput. Math. Methods Med. 4 (4), 223–239.

Schnarr, K., Dayes, I., Sathya, J., Boreham, D., 2007. Individual radiosensitivity and its relevance to health physics. Dose-Response 5 (4), dose–response.

Sotolongo-Grau, O., Rodriguez-Perez, D., Antoranz, J.C., Sotolongo-Costa, O., 2010. Tissue radiation response with maximum Tsallis entropy. Phys. Rev. Lett. 105 (15), 158105.

Sridharan, V., Margalit, D.N., Lynch, S.A., Severgnini, M., Zhou, J., Chau, N.G., Rabinowits, G., Lorch, J.H., Hammerman, P.S., Hodi, F.S., et al., 2016. Definitive chemoradiation alters the immunologic landscape and immune checkpoints in head and neck cancer. Br. J. Cancer 115 (2), 252.

Stylianopoulos, T., Martin, J.D., Chauhan, V.P., Jain, S.R., Diop-Frimpong, B., Bardeesy, N., Smith, B.L., Ferrone, C.R., Hornicek, F.J., Boucher, Y., Munn, L.L., R. K., J., 2012. Causes, consequences, and remedies for growth-induced solid stress in murine and human tumors. Proc. Natl. Acad. Sci. USA 109 (38), 15101–15108. doi:10.1073/pnas.1213353109.

Su, B., Zhou, W., Dorman, K.S., Jones, D.E., 2009. Mathematical modelling of immune response in tissues. Comput. Math. Methods Med. 10 (1), 9–38.

Thompson, M.K., Poortmans, P., Chalmers, A.J., Faivre-Finn, C., Hall, E., Huddart, R.A., Lievens, Y., Sebag-Montefiore, D., Coles, C.E., 2018. Practice-changing radiation therapy trials for the treatment of cancer: where are we 150 years after the birth of marie curie? Br. J. Cancer 119 (4), 389.

Walker, R., Poleszczuk, J., Pilon-Thomas, S., Kim, S., Anderson, A.A., Czerniecki, B.J., Harrison, L.B., Moros, E.G., Enderling, H., 2018. Immune interconnectivity of anatomically distant tumors as a potential mediator of systemic responses to local therapy. Sci. Rep. 8 (1), 9474.

Yang, T., 2001. Impulsive Control Theory, Vol. 272. Springer Science & Business Media.

Zlobec, I., Minoo, P., Karamitopoulou, E., Peros, G., Patsouris, E.S., Lehmann, F., Lugli, A., 2010. Role of tumor size in the pre-operative management of rectal cancer patients. BMC Gastroenterol. 10 (1), 61.